Journal of *Respiration*

MDPI

Article

Differential Effects of Oleuropein and Hydroxytyrosol on Aggregation and Stability of CFTR NBD1-ΔF508 Domain

Christopher S. Robinson [1,2,†], Jennifer A. Wyderko [1,3,†], Yeng Vang [1,4], Galen Martin [5,6] and Robert T. Youker [1,*]

1 Department of Biology, Western Carolina University, Cullowhee, NC 28723, USA; crobinson@pisgahlabs.com (C.S.R.); jwyderko@vt.edu (J.A.W.); yvang@exela.us (Y.V.)
2 Pisgah Labs, Pisgah Forest, NC 28768, USA
3 Office of Sponsored Programs, Virginia Tech, Blacksburg, VA 24060, USA
4 Exela Pharma Sciences, Lenoir, NC 28645, USA
5 Department of Biology, Warren Wilson College, Swannanoa, NC 28778, USA; galentm@uci.edu
6 Department of Ecology and Evolutionary Biology, University of California Irvine, Irvine, CA 92697, USA
* Correspondence: rtyouker@wcu.edu
† These authors contributed equally to this work.

Abstract: Cystic Fibrosis (CF) is caused by loss of function mutations in the Cystic Fibrosis transmembrane conductance regulator (CFTR). The folding and assembly of CFTR is inefficient. Deletion of F508 in the first nucleotide binding domain (NBD1-ΔF508) further disrupts protein stability leading to endoplasmic reticulum retention and proteasomal degradation. Stabilization and prevention of NBD1-ΔF508 aggregation is critical to rescuing the folding and function of the entire CFTR channel. We report that the phenolic compounds Oleuropein and Hydroxytryosol reduce aggregation of NBD1-ΔF508. The NBD1-ΔF508 aggregate size was smaller in the presence of Hydroxytryosol as determined by dynamic light scattering. Neither phenolic compound increased the thermal stability of NBD1-ΔF508 as measured by differential scanning fluorimetry. Interestingly, Hydroxytyrosol inhibited the stabilizing effect of the indole compound BIA, a known stabilizer, on NBD1-ΔF508. Molecular docking studies predicted that Oleuropein preferred to bind in the F1-type core ATP-binding subdomain in NBD1. In contrast, Hydroxytyrosol preferred to bind in the α4/α5/α6 helical bundle of the ABCα subdomain of NBD1 next to the putative binding site for BIA. This result suggests that Hydroxytyrosol interferes with BIA binding, thus providing an explanation for the antagonistic effect on NBD1 stability upon incubation with both compounds. To our knowledge, these studies are the first to explore the effects of these two phenolic compounds on the aggregation and stability of NBD1-ΔF508 domain of CFTR.

Keywords: CFTR; dynamic light scattering; NBD1-ΔF508; phenolic compounds

Citation: Robinson, C.S.; Wyderko, J.A.; Vang, Y.; Martin, G.; Youker, R.T. Differential Effects of Oleuropein and Hydroxytyrosol on Aggregation and Stability of CFTR NBD1-ΔF508 Domain. *J. Respir.* **2021**, *1*, 204–215. https://doi.org/10.3390/jor1030019

Academic Editors: Massimo Conese and Onofrio Laselva

Received: 11 May 2021
Accepted: 23 July 2021
Published: 4 August 2021

1. Introduction

The Cystic Fibrosis transmembrane conductance regulator (CFTR) gene encodes an ATP-binding cassette (ABC) transporter expressed in the apical membrane of epithelial cells that regulates chloride, bicarbonate, and water secretion. CFTR is composed of two nucleotide binding domains (NBD1, NBD2), two membrane spanning domains (MSD1, MSD2), and a unique regulatory domain (R). ATP-dependent "head-to-tail" heterodimerization of the NBDs and Phosphorylation of the R domain controls channel gating [1,2]. This complex multi-domain membrane protein requires an extensive proteo-stasis network for proper biogenesis and folding [3]. Mutations in the CFTR gene causes the autosomal recessive genetic disorder Cystic Fibrosis (CF) that affects >70,000 people worldwide [4–6]. Clinical manifestations of CF include pancreatic insufficiency, cardio-pulmonary impairment, digestive disfunction, liver disease, CF-related diabetes, and male infertility [7].

There are more than 2000 mutations identified in patients with CF but deletion of the amino acid phenylalanine at position 508 (ΔF508) in NBD1 domain of CFTR is present on

one or both alleles in 85–90% of patients [6]. The ΔF508 mutation causes global misfolding of CFTR leading to endoplasmic reticulum retention and proteasomal degradation [3,6]. The inefficient folding of CFTR-ΔF508 can be partially rescued through low temperature, revertant mutants, deletion of regulatory segment, chemical chaperones, and small molecule correctors, such as Lumacaftor [8–14]. The thermal stability, rate of folding, and solubility of NBD1 dictates the efficiency of folding and maturation of the entire CFTR protein [15–18]. It is believed that improved pharmacological correction of CFTR-ΔF508 will require targeting of multiple-domains (i.e., NBD1, NBD1-MSD2 interface, NBD2) and a critical target is stabilization of NBD1 [5,12,16,19–21].

The native fold of NBD1 is in equilibrium with a low-energy "molten-globule" conformation that has native-like secondary structure [22,23]. The ΔF508 mutation destabilizes the native conformation shifting the equilibrium to favor the molten-globule conformation that leads to robust aggregation in vitro. Binding of ATP to NBD1 can help to stabilize the native fold and prevent aggregation. In addition, multiple second-site mutations and chemical correctors have been identified that suppress formation of the molten-globule conformation caused by ΔF508 mutation and rescue the plasma membrane trafficking defect of CFTR [9–13,22–26]. This shift in the folding pathway is based on extensive thermodynamic analyses and is thought to occur through a "mass action" effect [15,23,24]. Therefore, extensive screens have been conducted over the years to identify molecules that can prevent aggregation and stabilize NBD1-ΔF508 [5].

Olive oil phenolic compounds possess anti-inflammatory, cardioprotective, neuroprotective, antioxidant, and anti-aggregatory activities [27]. Two compounds in olive oil that are important to these activities are Oleuropein and Hydroxytyrosol [27]. Oleuropein has been shown to inhibit amyloid (Aβ 1–42) aggregation in vitro and in vivo [28,29]. Oleuropein and Hydroxytyrosol both inhibit the aggregation of Tau [30]. In this study, we sought to determine if these two phenolic compounds could prevent the aggregation, and thermally stabilize the NBD1-ΔF508 domain of CFTR.

In this paper, we demonstrate that Oleuropein and Hydroxytyrosol suppress the aggregation of NBD1-ΔF508 in vitro. Furthermore, aggregate size is reduced in the presence of Hydroxytyrosol as measured by dynamic light scattering. The thermal stability of NBD1-ΔF508 is unaltered in the presence of Oleuropein and Hydroxytyrosol as determined by differential scanning fluorimetry. Interestingly, Hydroxytyrosol antagonizes the stabilizing effect of Bromoindole-3-acetic acid (BIA). Molecular docking studies predict that Hydroxytyrosol binds to similar surfaces as BIA and this may explain the antagonistic effect. To our knowledge, these studies are the first to explore the effects of these two phenolic compounds on the aggregation and stability of NBD1-ΔF508 domain of CFTR.

2. Materials and Methods

2.1. Compounds

Oleuropein and Hydroxytyrosol were purchased from Sigma (St. Louis, MO, USA) and were >98% pure. Bromoindole-3-acetic acid (BIA) was purchased from Sigma and was 97% pure. All compounds were dissolved in dried DMSO and stored at −20 °C.

2.2. mNBD1-ΔF508 Expression and Purification

Mouse NBD1-ΔF508 (residues G404-L644) was expressed and purified as described [31]. Briefly, BL21 (DE3) *E. coli* transformed with pET28a-mNBD1-ΔF508 plasmid were inoculated into 4 mL LB media containing 30 μg/mL kanamycin and grown overnight at 37 °C with vigorous shaking. The 4 mL saturated culture was diluted into 200 mL media and grown until OD_{600} ~0.60 then expression was induced with 1 mM isopropyl-1-thio-β-D-galacto-pyranoside for 3 h at 37 °C. Cells were harvested by centrifugation at 3200× *g* for 20 min at 4 °C and the cell pellet was resuspended in 40 mL buffer A (20 mM Tris-HCl pH 7.9, 500 mM NACl, 5 mM imidazole) plus protease inhibitors (cOmplete™ EDTA-free cocktail, Roche). Cells were lysed by sonication (3 × 30 s, 50 duty cycle) on ice and centrifuged for 30 min at 14,993× *g*. The post-sonicated pellet was resuspended in 5 mL

buffer A containing 6 M Guanidine hydrochloride (GdnHCl) and incubated on ice for 1 h. Resuspended pellet was centrifuged at 39,156× *g* for 20 min at 4 °C. Clarified lysate was incubated with 1–2 mL Ni-NTA resin (Qiagen) for 1 h on ice. Resin was washed sequentially with 10 mL buffer A with 6 M GdnHCl and 6 mL buffer A with 6 M GdnHCl and 20 mM imidazole. Protein was eluted with buffer A containing 6 M GdnHCl and 400 mM imidazole. Eluted protein was dialyzed against 2–4 L of 100 mM Tris-HCl pH 7.4 and 2 mM EDTA overnight at 4 °C. Precipitated protein was collected, dried and stored at −80 °C. The mNBD1-ΔF508 protein was ~90% pure based on densitometry of Coomassie stained gel.

2.3. Aggregation Assay

Purified mNBD1-ΔF508 (G404-L644) was resuspended in 100 µL of 6 M GdnHCl, 20 mM HEPES, pH 7.5 that yielded 28–37 µM protein based on 280 nm absorbance measurements. The resuspended protein was diluted to a final concentration of 2.5 µM in refolding buffer (100 mM Tris-HCl, pH 8, 385 mM L-arginine, 200 mM KCl, 20 mM $MgCl_2$, 1 mM DTT) and aggregation was monitored by turbidity (light scattering) at a wavelength of 400 nm at 35 °C in a Spectrovis-Plus Spectrophotometer (Vernier) in the absence or presence of the indicated concentrations of Oleuropein or Hydroxytyrosol. An equivalent amount of DMSO was used in the control experiments. Absorbance values were normalized to one using the control at the 40-min (Oleuropein) or 30-min (Hydroxytyrosol) timepoints. Experiments were performed with purified protein from at least two different preparations and two to five experiments per condition: Oleuropein control (n = 2), Oleuropein treatment (n = 4), Hydroxytyrosol control (n = 5), Hydroxytyrosol treatment (n = 4). Kinetic data was fitted to a four-parameter logistic equation to determine the inflection timepoint using Quest Graph™ Four Parameter Logistic (4PL) Curve Calculator.

2.4. Dynamic Light Scattering

Particle size was determined using a Malvern Zetasizer Nano ZS equipped with a 633 nm laser. Multiple ten-second scans were performed at room temperature and averaged for each run with dust filter algorithm enabled to remove noise. At the end of the aggregation assay (30-min timepoint), mNBD1-ΔF508 protein sample was transferred from the Spectrovis-Plus Spectrophotometer to the Zetasizer and average particle diameter and polydispersity index were measured. Three to four experiments with multiple replicates were performed: control (n = 4, 12 replicates), Hydroxytyrosol treatment (n = 3, 9 replicates).

2.5. Differential Scanning Fluorimetry

The Protein Thermal Shift Dye Kit (Applied Biosystems) was used according to manufacturer's protocol. All reactions were assembled either on ice or in a cold room at 4 °C. Either 2 µM or 5 µM of mNBD1-ΔF508 (residues T389-G673) was used in assays. The well plate was sealed with MicroAmp Optical Adhesive Film and spun at 1000 rpm for 1 min at 4 °C. A Melt curve experiment was performed with ROX reporter, no quencher, and continuous ramp mode on an ABI 7500 real-time PCR system.

Settings were Step 1 at 25 °C and a ramp rate of 100% (1.6 °C/s) for 2 min followed by Step 2 at 99 °C with 1% ramp rate (0.05 °C/s). Results were analyzed by the dman2.6 tool to extract melting point temperatures [32]. Experiments were performed three times and samples were run in triplicate.

2.6. Molecular Docking Simulations

Missing residues $_{414}$QSNGDRKHSSDENNV$_{428}$ residing in the regulatory insertion (RI) were added to the mNBD1-ΔF508 (PDB:3SI7) structure using MODELLER [33]. Five structures with modeled regions were generated and the model chosen for docking simulations had an −1.67 zDOPE score and estimated 1.190 Å RMSD (0.957 estimated overlap) with the original 3SI7 structure. The refined structure was uploaded to SwissDock for docking simulations [30]. Oleuropein and BIA molecule files were created in MOL2 file format

by the Dr. Lott Research group (WCU). Docking simulations of mouse NBD1-ΔF508 were performed with each individual ligand using Swissdock default settings. Swissdock uses CHARMM format EADock DSS software variant that loads 5000–15,000 binding modes and calculate the most favorable energies using the FACTS implicit solvent model [34]. Ligand coordinates were removed from consideration if exhibited any of the following: orientation of ligand away from NBD1, positive full fitness, or positive ΔG scores. Molecular visualization and graphics were performed using Chimera software.

2.7. Statistical Analysis

Data is expressed as mean ± SEM. Statistical differences between control and Oleuropein/Hydroxytyrosol treated samples were compared by unpaired t-test or ANOVA. Results were considered statistically significant if $p < 0.05$.

3. Results

3.1. Oleuropein and Hydroxytyrosol Suppress the Aggregation of mNBD1-ΔF508

We expressed and purified mouse NBD1-ΔF508 (mNBD1-ΔF508) from bacteria using immobilized metal affinity chromatography. This mNBD1 construct includes residues G404 to L644 and contains the F1-type core ATP-binding subdomain allowing the measurement of early folding intermediates (Figure 1A) [15,31,35]. Protein purity was ~90% based on gel densitometry (Figure 1B). Mouse NBD1-ΔF508 was chosen over human for experiments because to obtain experimentally useful quantities of human NBD1-ΔF508 requires multiple solubilization mutations and these mutations attenuate the ΔF508 defect and cause a two-fold prolonged gating cycle duration compared to wildtype [17,26,36,37]. Furthermore, deletion of the regulatory insertion overcomes solubility issues but also suppresses gating and trafficking defects of ΔF508 [10]. Importantly, purified mouse NBD1-ΔF508 has been used to probe Hsc70 interactions and successfully screen for pharmacological chaperones for human CFTR [13,38].

Purified mNBD1-ΔF508 (2.5 μM) was incubated with 100 μM Oleuropein (OLE) or Hydroxytyrosol (HT) and aggregation was monitored by light scattering using a spectrophotometer (see materials and methods). OLE and HT suppressed mNBD1-ΔF508 aggregation on average by 41 ± 6.9% and 34 ± 5.8%, at the terminal timepoint, respectively (Figure 1C,D). The calculated *p*-values for the observed differences in aggregation were 0.0348 (OLE) and 0.0017 (HT) compared to control. Incubation with ten-fold lower concentrations of OLE or HT (10 μM) inhibited aggregation to a similar extent (~30–40%) but results were inconsistent, with inhibition being observed only in half the experiments. In addition, aggregation was inhibited to the same extent with 200 μM OLE with a slight decrease in the inflection timepoint compared to 100 μM concentration (~11 vs. 14 min). Therefore, 100 μM of OLE and HT was chosen for the remainder of the experiments.

HT is naturally present in the brain as a by-product of dopamine and tyramine metabolism and is the major metabolite of OLE [27]. Therefore, we chose to further investigate the effects of 100 μM HT on mNBD1-ΔF508 aggregate/particle size using dynamic light scattering. The mNBD1-ΔF508 particle diameter was 1758 ± 235 and 1408 ± 207 nm for control and HT treated samples, respectively (Supplementary Figure S1A). The calculated *p*-value for the observed difference in diameters was 0.032. Both control and HT treated samples were significantly larger in average diameter compared to the 170 nm reference beads that were 176.9 ± 10.7 nm ($p = 7.17 \times 10^{-8}$ and 3.21×10^{-6}). There were larger aggregate species detected (~5×) for both control and HT treated samples but these represented a minority of the aggregate population (<10%) and there was no difference seen for these aggregates. The average polydispersity index for the 170 nm beads, control and HT treated aggregates were ~0.3 indicating the particles were homogeneous (Supplementary Figure S1B). There was a trend of increased polydispersity for the HT treated aggregates compared to control but this was not statistically significant.

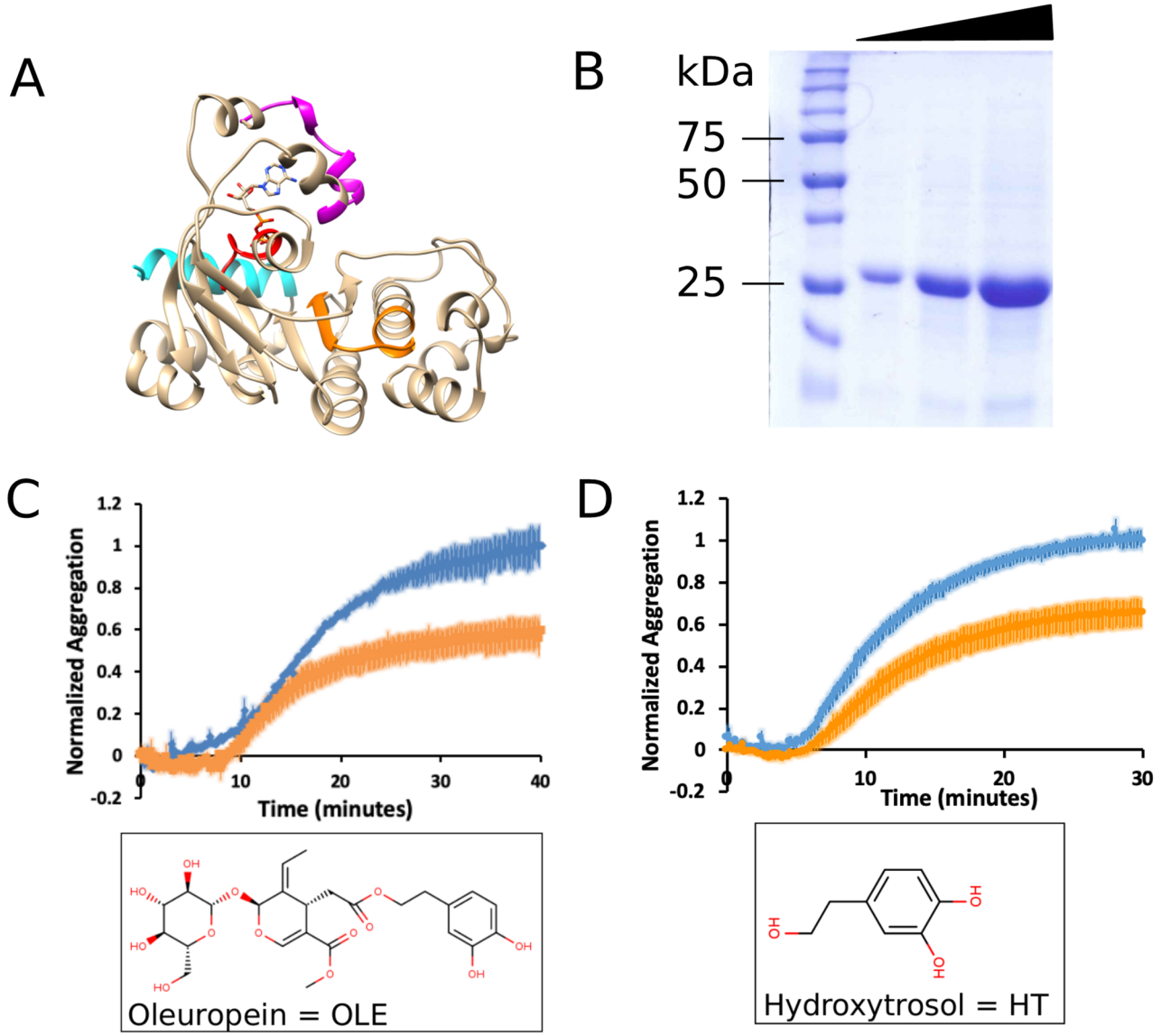

Figure 1. Oleuropein and Hydroxytyrosol suppress the aggregation of mNBD1-ΔF508 in vitro. (**A**) X-ray crystallographic structure of CFTR mNBD1 (PDB:3SI7) bound with ATP and relevant motifs highlighted: Walker A (red), W alker B (orange), regulatory extension (cyan), and regulatory insertion (magenta). (**B**) Coomassie stained gel of purified mNBD1-ΔF508 (residues 404–644) with increasing amounts of purified protein loaded (~5, 12, 25 µg). (**C**) Aggregation of 2.5 µM mNBD1-ΔF508 measured by light scattering in the absence (n = 2, blue) or presence of 100 µM Oleuropein (n = 4, orange), p-value = 0.0348. (**D**) Aggregation of 2.5 µM NBD1-ΔF508 in the absence (n = 5, blue) or presence of 100 µM Hydroxytyrosol (n = 4, orange), p-value = 0.0017. Absorbance values were normalized to control at the 40-min (Oleuropein) or 30-min (Hydroxytyrosol) timepoints. Data plotted as mean ± SEM.

3.2. Oleuropein and Hydroxytyrosol Do Not Thermally Stabilize mNBD1-ΔF508

Since OLE and HT prevented aggregation of mNBD1-ΔF508, we employed differential scanning fluorimetry (DSF) to determine if these polyphenolic compounds could also thermally stabilize the protein (see materials and methods). It is known that ATP and 5-Bromoindole-3-acetic acid (BIA) molecules bind and thermally stabilize NBD1 in vitro [12,18,39]. Therefore, both molecules were used as positive controls in our DSF assays. For DSF experiments, we employed a NBD1-ΔF508 construct spanning residues T389-G673 in order to allow a more direct comparison with previous studies that investigated mNBD1 thermal stability [13]. In addition, this construct contains the regulatory extension that can obstruct head–tail homodimer formation and thus would minimize

potential dimerization contribution to stability measurements [40]. The T_m of mNBD1-ΔF508 was 29.97 ± 0.32 °C and incubation with 1- or 5-mM ATP increased the average Tm by +3.73 ± 0.64 °C and +5.93 ± 0.05 °C similar to previous reports for mouse and human NBD1-ΔF508 [12,13,18,39] (Figure 2A and Table 1). The calculated *p*-values ($p_{1\ mM\ ATP}$ = 0.00275, $p_{5\ mM\ ATP}$ = 0.00006) indicated the difference in melting temperature in the presence of the two ATP concentrations were statistically significant. In addition, 1 mM BIA increased NBD1's thermal stability by an average of +2.13 ± 0.16 °C (p = 0.030) similar to a previous report (Figure 2C) [18].

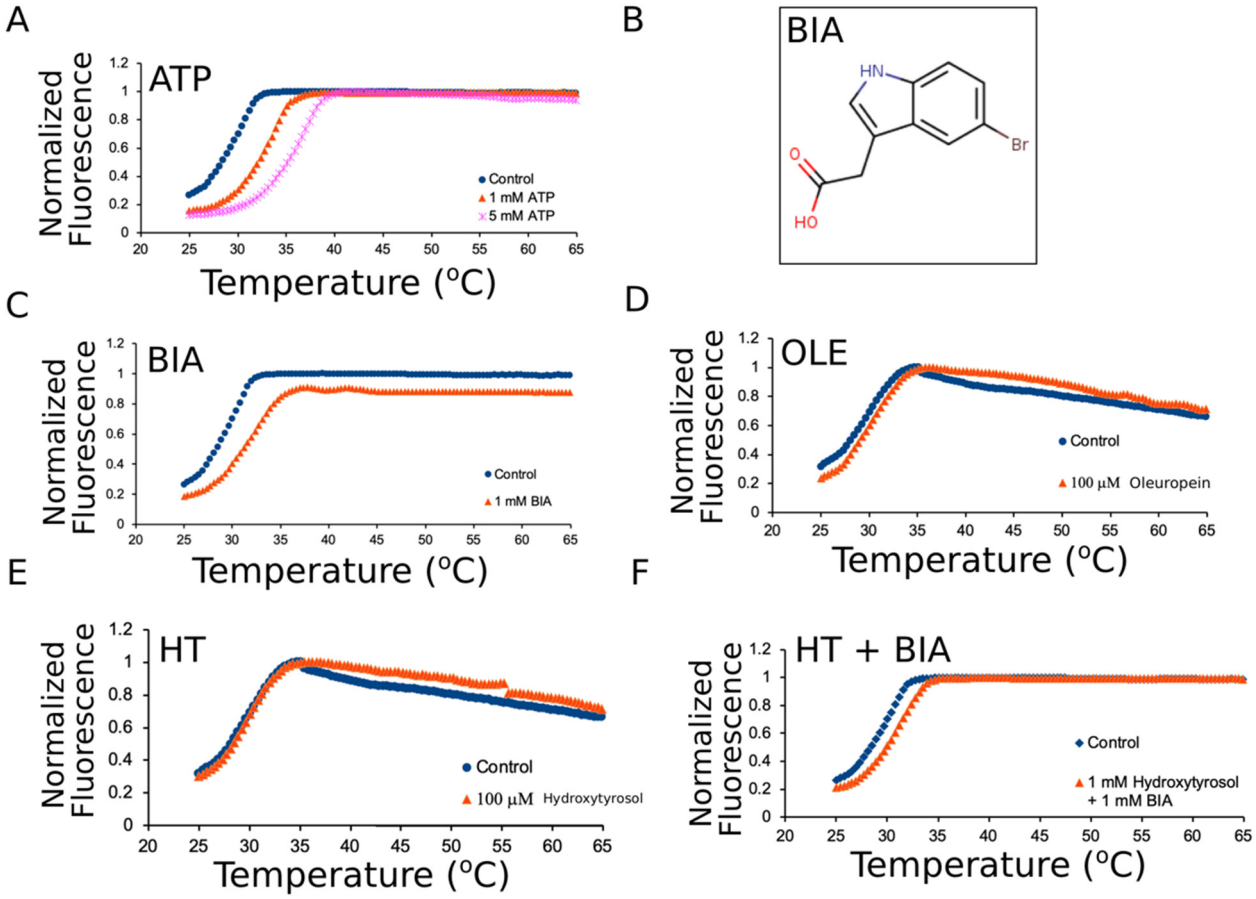

Figure 2. Oleuropein and Hydroxytyrosol do not affect thermal stability of mNBD1-ΔF508. (**A**) mNBD1-ΔF508 thermal stability measured in absence (blue), or presence of 1 mM or 5 mM ATP (orange or pink) using differential scanning fluorimetry, *p*-value = 0.00275 and 0.00006, respectively. (**B**) Structure of 5-*bromoindole*-3-acetic acid (BIA) compound used in experiments. (**C**) mNBD1-ΔF508 thermal stability measured in absence (blue), or presence of 1 mM BIA (orange), *p*-value = 0.03006. (**D**) mNBD1-ΔF508 thermal stability measured in absence (blue), or presence of 100 µM Oleuropein (orange), *p*-value = 0.6167. (**E**) mNBD1-ΔF508 thermal stability measured in absence (blue), or presence of 100 µM Hydroxytyrosol (orange), *p*-value = 0.7999. (**F**) mNBD1-ΔF508 thermal stability measured in absence (blue), or presence of 1 mM Hydroxytyrosol and 1 mM BIA (orange), *p*-value = 0.02076. Representative curves presented (n = 3 and 3 replicates per experiment) and significant differences were analyzed by ANOVA.

NBD1-ΔF508 was incubated with both ATP (1.5 mM) and BIA (1 mM) to determine if their effects are synergistic, or not. The multiple ligands increased thermal stability by 5.67 ± 0.21 °C and was statistically significant (p = 0.00015). This result suggests that multiple ligands combined can provide a synergistic effect on thermal stability of NBD1-ΔF508. This result is similar to the additive effects of MCG1516A, RDR1, VX809 in the presence of ATP that were reported to stabilize human NBD1-ΔF508 [21].

Table 1. Summary of DSF experiments of mNBD1-ΔF508 with/without ligands.

Groups	Average °C	Variance
mNBD1-ΔF508	29.97	0.32
mNBD1-ΔF508 + 1 mM ATP	33.70	0.64
mNBD1-ΔF508 + 5 mM ATP	36.13	0.05
mNBD1-ΔF508 + 1 mM BIA	32.10	0.16
mNBD1-ΔF508 + 1.5 mM ATP + 1 mM BIA	35.87	0.21
mNBD1-ΔF508 + 100 μM Oleuropein	30.23	0.40
mNBD1-ΔF508 + 100 μM Hydroxy-Tyrosol	29.83	0.40
mNBD1-ΔF508 + 500 μM Hydroxy-Tyrosol	29.73	0.16
mNBD1-ΔF508 + 1 mM Hydroxy-Tyrosol	29.47	0.56
mNBD1-ΔF508 + 1 mM Hydroxy-Tyrosol + 1 mM BIA	31.53	0.21

OLE (100 μM) increased thermal stability of NBD1-ΔF508 by +0.26 °C, but this was not deemed statistically significant (p = 0.61671) (Figure 2D). HT tested at 100 μM also did not affect NBD1-ΔF508 thermal stability. We tested 5× and 10× higher concentrations of HT, 500 μM to 1 mM, and confirmed there was no significant change in the protein T_m (p = 0.799 and 0.593) (Figure 2E). Interestingly, incubation of 1 mM HT combined with 1 mM BIA increased thermal stability by +1.56 ± 0.21 °C but the results were decreased compared to 1 mM BIA alone, suggesting an antagonist effect exerted by HT (p = 0.02076) (Figure 2F).

3.3. Predicted Molecular Docking of BIA, Oleuropein, and Hydroxytryosol to mNBD1-ΔF508

We performed molecular docking studies to gain insight into the apparent antagonist effect of HT on BIA induced thermal stabilization of mNBD1-ΔF508. BIA, OLE, and HT were computationally bound to mNBD1-ΔF508 using Swissdock (Table S1) [34]. Multiple binding modes were identified for BIA and one predicted binding site was in a cleft between the ABCα and F1-type core ATP-binding subdomains near the apex of the α4/α5/α6 helical bundle (Figure 3A and Figure S2A). This predicted site is very close to the binding site determined from co-crystallization experiments performed by SGX pharmaceuticals and is termed the α-site [18]. In contrast to BIA, OLE only had two predicted binding modes, or surface next to the site of ATP binding in the F1-type core ATP-binding subdomain (Figure 3B and Figure S2B). There were many predicted binding modes for HT but the majority of the predicted clusters were in the α4/α5/α6 helical bundle of the ABCα subdomain (Figure 3C and Figure S2C). Interestingly, many of the predicted binding modes for HT overlapped or were in close opposition (2–12 Å) to the predicted BIA modes, including sites in the ABCα-, ABCβ-subdomain (also known as α/β-subdomain) and the regulatory extension region (Figure S2A,C). Overall, these docking results suggest that HT binds to a region near the α-site and this could interfere with BIA binding (Figure 3C).

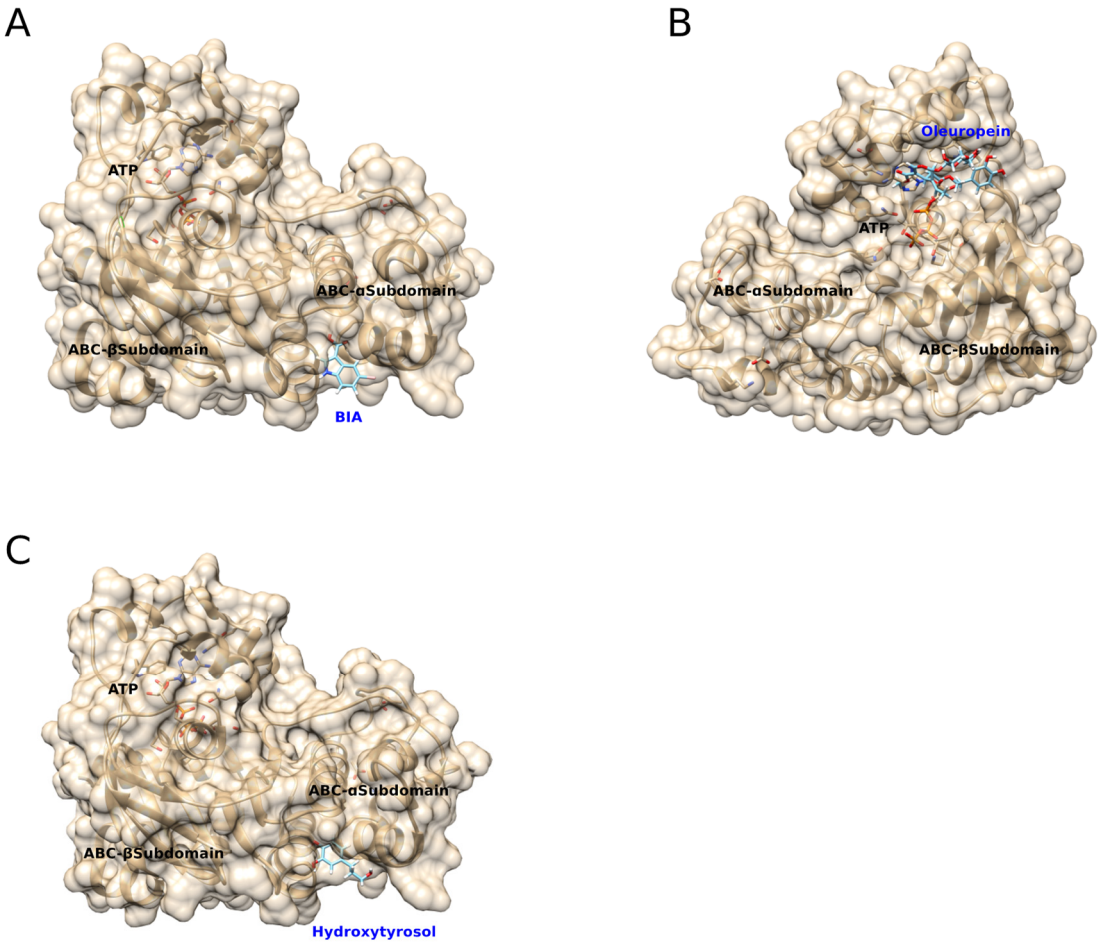

Figure 3. Predicted Binding of BIA, Oleuropein, and Hydroxytyrosol to mNBD1-ΔF508. SwissDock was used to predict binding modes between BIA (**A**) Oleuropein (**B**) and Hydroxytyrosol (**C**) with mNBD1-ΔF508 (PDB:3SI7). Docking results for the highest scored complexes for BIA, Oleuropein, and Hydroxytyrosol are shown (see Materials and Methods).

4. Discussion

The antioxidants OLE and HT suppressed the aggregation but did not alter the thermal stability of mNBD1-ΔF508. Our kinetic data was sigmoidal shaped suggesting that aggregation occurred through a nucleation-growth process [41]. We fitted the aggregation data with a four-parameter logistic regression to determine the maximum aggregation rate for control versus treated conditions (i.e., inflection parameter). There was no significant difference between the average inflection values for control (10.94 $\pm$ 0.54 min) compared to HT (11.67 $\pm$ 0.68 min), and control (16.75 $\pm$ 0.90 min) compared to OLE (14.38 $\pm$ 0.77 min) treatments, respectively (Figure S3). The plateau phase of aggregation but not the lag phase and initial growth were affected by OLE and HT. Interestingly, there was a significant difference between the inflection values for OLE and HT treatments (p = 0.019479).

Together with our DLS measurements (Figure 2 and Table S2), these results suggest that growth but not initial formation of aggregates is suppressed, resulting in a modest reduction of overall aggregate size. This alteration of aggregate size could be due to prevention of monomer addition or disruption of aggregates. One possibility is that OLE and HT are shifting the equilibrium to disfavor the "molten-globule" aggregation prone conformer. Our data is consistent with the model of Omar et al. who investigated Aβ fibril formation and proposed that olive oil polyphenols inhibit protein aggregation through breakdown of pre-formed aggregates [42]. Our data is also consistent with Daccache et al., who observed less total aggregated material when Tau or Tau-P301L were incubated with OLE and HT [30].

The indole-based compound BIA increased mNBD1-ΔF508 stability by an average of 2.13 °C and this was similar to He et al.'s reported value of 1.4 °C [18]. Interestingly, He and colleagues incubated their NBD1 constructs with 4× higher BIA concentration (4 mM vs. 1 mM) to observe a similar stabilization compared to our study. The mNBD1-ΔF508 construct, used in our studies, contains the naturally disordered RI region (residues 405–436) compared to He [18]. A second difference is that He used human NBD1 in their studies compared to mouse in our experiments. However, the average T_m of our mNBD1-ΔF508 (residues 389–673) was ~30 °C compared to 30–31 °C for human NBD1-ΔF508 (residues 389–678) as previously reported [12,19]. The concentration differences between our and He et al.'s results are most likely due to the inclusion/omission of the RI region.

These phenolic compounds suppress Tau, α-synuclein, and Aβ fibrillation with low micromolar IC_{50} concentrations (2–36 μM) and close to 1:1 molar ratio [30,43,44]. In contrast, a 1:40 molar ratio (100 μM) of OLE and HT was required to suppress mNBD1-ΔF508 aggregation. In our hands, a lower concentration of 10 μM (1:4 molar ratio) gave inconsistent results in suppressing aggregation. Biochemical studies suggest both covalent and non-covalent interactions are believed to contribute to the HT mediated prevention of aggregation [43]. The concentration differences we observed could imply that the covalent binding of OLE and HT to NBD1-ΔF508 is very weak, or that non-covalent interactions predominate (see below).

OLE and HT have been reported to suppress the aggregation of Tau and Aβ aggregation in vitro and in vivo [29,30]. Recent biophysical studies suggest that the mechanism of aggregation prevention for OLE and HT are fundamentally different [43,44]. For example, Oleuropein aglycone (de-glycosylated Oleuropein) appears to block $Aβ_{1–42}$ fibril growth through binding to the N-terminus of the peptide [44]. In contrast, HT appears to increase the rate of harmless off-pathway amorphous aggregates [44]. The HT molecule may exert this effect through stabilization of specific regions of the protein [43]. Our molecular docking results predicted that OLE binds preferentially in the ATP binding pocket and HT preferentially binds to the ABCα-subdomain. Interestingly, HT partially inhibited the stabilizing effect of BIA and this predicted interference could be caused by HT stabilization of an NBD1-ΔF508 conformation that disrupts BIA binding or competes for a similar binding site as predicted by our docking studies.

Recently, several nanobodies were discovered to bind to the top of the Walker A motif in a small cavity in the β-subdomain that overlaps with the regulatory insertion packing of NBD1 (Figure 1A) [45]. The predicted binding modes for OLE are also in the β-subdomain but these sites are between ~15–25 angstroms away from the nanobody binding surface and thus would not likely interfere. Interestingly, several of the predicted binding modes for HT in the β-subdomain are ~6.5 angstroms from G550 and ~7.20 angstroms from S605. Both of these residues participate in polar interactions with the nanobodies to facilitate binding [45]. Therefore, the predicted HT binding sites could interfere with the binding of the nanobodies to NBD1 and potentially abrogate the thermal stabilization observed by Sigoillet et al. [45].

Several nucleotide analogs, including dTTP, are known to bind with higher affinity to the same site as ATP in NBD1 and restore ΔF508-CFTR electrophysiological function [22]. The predicted binding sites for OLE are near the ATP pocket. In contrast, the HT and BIA predicted binding sites are not near the ATP pocket. Interestingly, lower scoring binding modes for OLE, HT and BIA located in between the two subdomains could interfere with residues at the NBD1-NBD2 dimerization interface (Figure S2) [46]. Correctors known to restore the intracellular loop 4 (ICL4) interaction with NBD1 by either direct binding to the ΔF508 loop or through indirect allosteric effects are not predicted to be affected by OLE or HT binding based on our docking studies [47–49]. Importantly, binding to remote sites (removed from F508) in NBD1 can lead to allosteric changes and stabilization. The predicted neutral or negative impacts of OLE or HT, described above, would need to be verified experimentally through a technique such as hydrogen/deuterium exchange mass spectrometry [49]. Overall, OLE and HT would be predicted to have limited potential as a

corrector or potentiator due to the high concentrations needed for their effect, inability to stabilize NBD1-ΔF508, and the predicted interference with NBD1-NBD2 dimerization, and correctors (such as BIA and nanobodies). Additional biophysical studies will be needed to fully understand the anti-aggregatory activities of these phenolic compounds towards mNBD1 and to test these predictions. Finally, future lab efforts will be directed towards characterization of the aggregate geometry and morphology in the presence of OLE and HT using electron microscopy techniques (TEM/SEM/AFM).

Supplementary Materials: The following are available online at https://www.mdpi.com/article/10.3390/jor1030019/s1, Table S1: Ligand-mNBD1-ΔF508 docking scores of BIA and Oleuropein full fitness and ΔG values for most stable docked molecules shown in Figure 3, Table S2: ANOVA analysis of DSF experiments, Figure S1: NBD1−ΔF508 aggregates incubated with Hydroxytyrosol are smaller in diameter and mostly monodispersed, Figure S2: Full SwissDock predicted binding modes for BIA, Oleuropein, and Hydroxytyrosol to mNBD1−ΔF508. Figure S3: Curve fitting of mNBD1-F508 aggregation data from Figure 1C,D.

Author Contributions: C.S.R.: Investigation, Methodology, Validation, Writing-Reviewing and Editing. J.A.W.: Investigation, Methodology, Writing—Reviewing and Editing. Y.V.: Investigation, Writing—Reviewing and Editing. G.M.: Investigation, Writing—Reviewing and Editing R.T.Y.: Conceptualization, Methodology, Supervision, Writing—Original Draft and Editing. All authors have read and agreed to the published version of the manuscript.

Funding: This research received no external funding.

Data Availability Statement: All data is contained within article and Supplementary Materials.

Acknowledgments: We thank Philip Thomas (UT Southwestern) for the gift of plasmid pET28a-NBD1-ΔF508 (residues G404-L644) and murine NBD1-ΔF508 protein. The Zetasizer instrument was funded by a Grant from the North Carolina Biotechnology Center (Western Carolina University, P.I. Evanoff).

Conflicts of Interest: The authors declare no conflict of interest.

References

1. Mense, M.; Vergani, P.; White, D.M.; Altberg, G.; Nairn, A.C.; Gadsby, D.C. In vivo phosphorylation of CFTR promotes formation of a nucleotide-binding domain heterodimer. *EMBO J.* **2006**, *25*, 4728–4739. [CrossRef]
2. Csanády, L.; Nairn, A.; Gadsby, D.C. Thermodynamics of CFTR Channel Gating: A Spreading Conformational Change Initiates an Irreversible Gating Cycle. *J. Gen. Physiol.* **2006**, *128*, 523–533. [CrossRef]
3. Estabrooks, S.; Brodsky, J.L. Regulation of CFTR Biogenesis by the Proteostatic Network and Pharmacological Modulators. *Int. J. Mol. Sci.* **2020**, *21*, 452. [CrossRef]
4. Riordan, J.R.; Rommens, J.M.; Kerem, B.; Alon, N.; Rozmahel, R.; Grzelczak, Z.; Zielenski, J.; Lok, S.; Plavsic, N.; Chou, J.L.; et al. Identification of the cystic fibrosis gene: Cloning and characterization of complementary DNA. *Science* **1989**, *245*, 1066–1073. [CrossRef]
5. Lopes-Pacheco, M. CFTR Modulators: Shedding Light on Precision Medicine for Cystic Fibrosis. *Front. Pharmacol.* **2016**, *7*, 275. [CrossRef] [PubMed]
6. The Clinical and Functional TRanslation of CFTR (CFTR2). Available online: http://cftr2.org (accessed on 24 July 2020).
7. Castellani, C.; Assael, B.M. Cystic fibrosis: A clinical view. *Cell. Mol. Life Sci.* **2016**, *74*, 129–140. [CrossRef]
8. Denning, G.; Anderson, M.; Amara, J.F.; Marshall, J.; Smith, A.E.; Welsh, M. Processing of mutant cystic fibrosis transmembrane conductance regulator is temperature-sensitive. *Nature* **1992**, *358*, 761–764. [CrossRef] [PubMed]
9. Teem, J.L.; Berger, H.; Ostedgaard, L.; Rich, D.P.; Tsui, L.-C.; Welsh, M. Identification of revertants for the cystic fibrosis ΔF508 mutation using STE6-CFTR chimeras in yeast. *Cell* **1993**, *73*, 335–346. [CrossRef]
10. Aleksandrov, A.A.; Kota, P.; Aleksandrov, L.A.; He, L.; Jensen, T.; Cui, L.; Gentzsch, M.; Dokholyan, N.V.; Riordan, J.R. Regulatory Insertion Removal Restores Maturation, Stability and Function of ΔF508 CFTR. *J. Mol. Biol.* **2010**, *401*, 194–210. [CrossRef] [PubMed]
11. Farinha, C.; King-Underwood, J.; Sousa, M.; Correia, A.R.; Henriques, B.; Roxo-Rosa, M.; Da Paula, A.C.; Williams, J.; Hirst, S.; Gomes, C.M.; et al. Revertants, Low Temperature, and Correctors Reveal the Mechanism of F508del-CFTR Rescue by VX-809 and Suggest Multiple Agents for Full Correction. *Chem. Biol.* **2013**, *20*, 943–955. [CrossRef]
12. Okiyoneda, T.; Veit, G.; Dekkers, J.F.; Bagdany, M.; Soya, N.; Xu, H.; Roldan, A.; Verkman, A.S.; Kurth, M.J.; Simon, A.; et al. Mechanism-based corrector combination restores ΔF508-CFTR folding and function. *Nat. Chem. Biol.* **2013**, *9*, 444–454. [CrossRef]

13. Sampson, H.M.; Robert, R.; Liao, J.; Matthes, E.; Carlile, G.W.; Hanrahan, J.W.; Thomas, D. Identification of a NBD1-Binding Pharmacological Chaperone that Corrects the Trafficking Defect of F508del-CFTR. *Chem. Biol.* **2011**, *18*, 231–242. [CrossRef]
14. Van Goor, F.; Hadida, S.; Grootenhuis, P.D.J.; Burton, B.; Stack, J.H.; Straley, K.S.; Decker, C.J.; Miller, M.; McCartney, J.; Olson, E.R.; et al. Correction of the F508del-CFTR protein processing defect in vitro by the investigational drug VX-809. *Proc. Natl. Acad. Sci. USA* **2011**, *108*, 18843–18848. [CrossRef]
15. Qu, B.-H.; Thomas, P.J. Alteration of the Cystic Fibrosis Transmembrane Conductance Regulator Folding Pathway: Effects of the Δf508 Mutation on the Thermodynamic Stability and Folding Yield of Nbd1. *J. Biol. Chem.* **1996**, *271*, 7261–7264. [CrossRef]
16. Mendoza, J.; Schmidt, A.; Li, Q.; Nuvaga, E.; Barrett, T.; Bridges, R.J.; Feranchak, A.P.; Brautigam, C.; Thomas, P.J. Requirements for Efficient Correction of ΔF508 CFTR Revealed by Analyses of Evolved Sequences. *Cell* **2012**, *148*, 164–174. [CrossRef]
17. Yang, Z.; Hildebrandt, E.; Jiang, F.; Aleksandrov, A.A.; Khazanov, N.; Zhou, Q.; An, J.; Mezzell, A.; Xavier, B.M.; Ding, H.; et al. Structural stability of purified human CFTR is systematically improved by mutations in nucleotide binding domain 1. *Biochim. Biophys. Acta Biomembr.* **2018**, *1860*, 1193–1204. [CrossRef] [PubMed]
18. He, L.; Aleksandrov, A.A.; An, J.; Cui, L.; Yang, Z.; Brouillette, C.G.; Riordan, J.R. Restoration of NBD1 Thermal Stability Is Necessary and Sufficient to Correct ΔF508 CFTR Folding and Assembly. *J. Mol. Biol.* **2015**, *427*, 106–120. [CrossRef] [PubMed]
19. Rabeh, W.; Bossard, F.; Xu, H.; Okiyoneda, T.; Bagdany, M.; Mulvihill, C.M.; Du, K.; di Bernardo, S.; Liu, Y.; Konermann, L.; et al. Correction of Both NBD1 Energetics and Domain Interface Is Required to Restore ΔF508 CFTR Folding and Function. *Cell* **2012**, *148*, 150–163. [CrossRef] [PubMed]
20. Micoud, J.; Chauvet, S.; Scheckenbach, K.E.L.; Alfaidy, N.; Chanson, M.; Benharouga, M.; Julien, M. Involvement of the heterodimeric interface region of the nucleotide binding domain-2 (NBD2) in the CFTR quaternary structure and membrane stability. *Biochim. Biophys. Acta Mol. Cell Res.* **2015**, *1853*, 2420–2431. [CrossRef]
21. Carlile, G.W.; Yang, Q.; Matthes, E.; Liao, J.; Radinovic, S.; Miyamoto, C.; Robert, R.; Hanrahan, J.W.; Thomas, D.Y. A novel triple combination of pharmacological chaperones improves F508del-CFTR correction. *Sci. Rep.* **2018**, *8*, 1–16. [CrossRef] [PubMed]
22. Wang, C.; Aleksandrov, A.A.; Yang, Z.; Forouhar, F.; Proctor, E.A.; Kota, P.; An, J.; Kaplan, A.; Khazanov, N.; Boël, G.; et al. Ligand binding to a remote site thermodynamically corrects the F508del mutation in the human cystic fibrosis transmembrane conductance regulator. *J. Biol. Chem.* **2018**, *293*, 17685–17704. [CrossRef]
23. Protasevich, I.; Yang, Z.; Wang, C.; Atwell, S.; Zhao, X.; Emtage, S.; Wetmore, D.; Hunt, J.F.; Brouillette, C.G. Thermal unfolding studies show the disease causing F508del mutation in CFTR thermodynamically destabilizes nucleotide-binding domain 1. *Protein Sci.* **2010**, *19*, 1917–1931. [CrossRef]
24. Wang, C.; Protasevich, I.; Yang, Z.; Seehausen, D.; Skalak, T.; Zhao, X.; Atwell, S.; Emtage, J.S.; Wetmore, D.R.; Brouillette, C.G.; et al. Integrated biophysical studies implicate partial unfolding of NBD1 of CFTR in the molecular pathogenesis of F508del cystic fibrosis. *Protein Sci.* **2010**, *19*, 1932–1947. [CrossRef]
25. Ptitsyn, O.; Pain, R.; Semisotnov, G.; Zerovnik, E.; Razgulyaev, O. Evidence for a molten globule state as a general intermediate in protein folding. *FEBS Lett.* **1990**, *262*, 20–24. [CrossRef]
26. Pissarra, L.S.; Farinha, C.; Xu, Z.; Schmidt, A.; Thibodeau, P.; Cai, Z.; Thomas, P.J.; Sheppard, D.N.; Amaral, M.D. Solubilizing Mutations Used to Crystallize One CFTR Domain Attenuate the Trafficking and Channel Defects Caused by the Major Cystic Fibrosis Mutation. *Chem. Biol.* **2008**, *15*, 62–69. [CrossRef] [PubMed]
27. Marković, A.K.; Torić, J.; Barbarić, M.; Brala, C.J. Hydroxytyrosol, Tyrosol and Derivatives and Their Potential Effects on Human Health. *Molecules* **2019**, *24*, 2001. [CrossRef]
28. Rigacci, S.; Guidotti, V.; Bucciantini, M.; Nichino, D.; Relini, A.; Berti, A.; Stefani, M. Aβ(1-42) Aggregates into Non-Toxic Amyloid Assemblies in the Presence of the Natural Polyphenol Oleuropein Aglycon. *Curr. Alzheimer Res.* **2011**, *8*, 841–852. [CrossRef] [PubMed]
29. Diomede, L.; Rigacci, S.; Romeo, M.; Stefani, M.; Salmona, M. Oleuropein Aglycone Protects Transgenic *C. elegans* Strains Expressing Aβ42 by Reducing Plaque Load and Motor Deficit. *PLoS ONE* **2013**, *8*, e58893. [CrossRef]
30. Daccache, A.; Lion, C.; Sibille, N.; Gérard, M.; Slomianny, C.; Lippens, G.; Cotelle, P. Oleuropein and derivatives from olives as Tau aggregation inhibitors. *Neurochem. Int.* **2011**, *58*, 700–707. [CrossRef]
31. Youker, R.; Walsh, P.; Beilharz, T.; Lithgow, T.; Brodsky, J.L. Distinct Roles for the Hsp40 and Hsp90 Molecular Chaperones during Cystic Fibrosis Transmembrane Conductance Regulator Degradation in Yeast. *Mol. Biol. Cell* **2004**, *15*, 4787–4797. [CrossRef]
32. Wang, C.K.; Weeratunga, S.; Pacheco, C.M.; Hofmann, A. DMAN: A Java tool for analysis of multi-well differential scanning fluorimetry experiments. *Bioinformatics* **2011**, *28*, 439–440. [CrossRef]
33. Šali, A.; Blundell, T.L. Comparative Protein Modelling by Satisfaction of Spatial Restraints. *J. Mol. Biol.* **1993**, *234*, 779–815. [CrossRef]
34. Grosdidier, A.; Zoete, V.; Michielin, O. SwissDock, a protein-small molecule docking web service based on EADock DSS. *Nucleic Acids Res.* **2011**, *39*, W270–W277. [CrossRef] [PubMed]
35. Strickland, E.; Qu, B.-H.; Millen, L.; Thomas, P.J. The Molecular Chaperone Hsc70 Assists the in VitroFolding of the N-terminal Nucleotide-binding Domain of the Cystic Fibrosis Transmembrane Conductance Regulator. *J. Biol. Chem.* **1997**, *272*, 25421–25424. [CrossRef] [PubMed]
36. Lewis, H.A.; Buchanan, S.G.; Burley, S.K.; Conners, K.; Dickey, M.; Dorwart, M.; Fowler, R.; Gao, X.; Guggino, W.B.; Hendrickson, W.A.; et al. Structure of nucleotide-binding domain 1 of the cystic fibrosis transmembrane conductance regulator. *EMBO J.* **2003**, *23*, 282–293. [CrossRef]

37. Baker, J.M.R.; Hudson, R.P.; Kanelis, V.; Choy, W.-Y.; Thibodeau, P.H.; Thomas, P.J.; Forman-Kay, J.D. CFTR regulatory region interacts with NBD1 predominantly via multiple transient helices. *Nat. Struct. Mol. Biol.* **2007**, *14*, 738–745. [CrossRef] [PubMed]
38. Scott-Ward, T.S.; Amaral, M.D. Deletion of Phe508 in the first nucleotide-binding domain of the cystic fibrosis transmembrane conductance regulator increases its affinity for the heat shock cognate 70 chaperone: Interaction of Hsc70 with F508del-NBD1. *FEBS J.* **2009**, *276*, 7097–7109. [CrossRef]
39. Hall, J.D.; Wang, H.; Byrnes, L.J.; Shanker, S.; Wang, K.; Efremov, I.V.; Chong, P.A.; Forman-Kay, J.D.; Aulabaugh, A.E. Binding screen for cystic fibrosis transmembrane conductance regulator correctors finds new chemical matter and yields insights into cystic fibrosis therapeutic strategy: CFTR Correctors in CF Therapeutics. *Protein Sci.* **2016**, *25*, 360–373. [CrossRef]
40. Atwell, S.; Brouillette, C.G.; Conners, K.; Emtage, S.; Gheyi, T.; Guggino, W.B.; Hendle, J.; Hunt, J.F.; Lewis, H.A.; Lu, F.; et al. Structures of a minimal human CFTR first nucleotide-binding domain as a monomer, head-to-tail homodimer, and pathogenic mutant. *Protein Eng. Des. Sel.* **2010**, *23*, 375–384. [CrossRef]
41. Zapadka, K.L.; Becher, F.J.; Dos Santos, A.L.G.; Jackson, S.E. Factors affecting the physical stability (aggregation) of peptide therapeutics. *Interface Focus* **2017**, *7*, 20170030. [CrossRef]
42. Omar, S.H.; Scott, C.J.; Hamlin, A.S.; Obied, H.K. Olive Biophenols Reduces Alzheimer's Pathology in SH-SY5Y Cells and APPswe Mice. *Int. J. Mol. Sci.* **2018**, *20*, 125. [CrossRef]
43. Palazzi, L.; Leri, M.; Cesaro, S.; Stefani, M.; Bucciantini, M.; de Laureto, P.P. Insight into the molecular mechanism underlying the inhibition of α-synuclein aggregation by hydroxytyrosol. *Biochem. Pharmacol.* **2020**, *173*, 113722. [CrossRef] [PubMed]
44. Leri, M.; Natalello, A.; Bruzzone, E.; Stefani, M.; Bucciantini, M. Oleuropein aglycone and hydroxytyrosol interfere differently with toxic Aβ1-42 aggregation. *Food Chem. Toxicol.* **2019**, *129*, 1–12. [CrossRef]
45. Sigoillot, M.; Overtus, M.; Grodecka, M.; Scholl, D.; Garcia-Pino, A.; Laeremans, T.; He, L.; Pardon, E.; Hildebrandt, E.; Urbatsch, I.; et al. Domain-interface dynamics of CFTR revealed by stabilizing nanobodies. *Nat. Commun.* **2019**, *10*, 2636. [CrossRef] [PubMed]
46. Kalid, O.; Mense, M.; Fischman, S.; Shitrit, A.; Bihler, H.; Ben-Zeev, E.; Schutz, N.; Pedemonte, N.; Thomas, P.J.; Bridges, R.J.; et al. Small molecule correctors of F508del-CFTR discovered by structure-based virtual screening. *J. Comput. Mol. Des.* **2010**, *24*, 971–991. [CrossRef] [PubMed]
47. Hudson, R.P.; Dawson, J.E.; Chong, P.A.; Yang, Z.; Millen, L.; Thomas, P.J.; Brouillette, C.G.; Forman-Kay, J.D. Direct Binding of the Corrector VX-809 to Human CFTR NBD1: Evidence of an Allosteric Coupling between the Binding Site and the NBD1:CL4 Interface. *Mol. Pharmacol.* **2017**, *92*, 124–135. [CrossRef] [PubMed]
48. Bitam, S.; Elbahnsi, A.; Creste, G.; Pranke, I.; Chevalier, B.; Berhal, F.; Hoffmann, B.; Servel, N.; Tondelier, D.; Hatton, A.; et al. New insights into structure and function of bis-phosphinic acid derivatives and implications for CFTR modulation. *Sci. Rep.* **2021**, *11*, 6842. [CrossRef] [PubMed]
49. Byrnes, L.J.; Xu, Y.; Qiu, X.; Hall, J.D.; West, G.M. Sites associated with Kalydeco binding on human Cystic Fibrosis Transmembrane Conductance Regulator revealed by Hydrogen/Deuterium Exchange. *Sci. Rep.* **2018**, *8*, 4664. [CrossRef]